Photoelectron spectra and structure of the Mn n − anions (n = 2–16)

G. L. Gutsev, C. A. Weatherford, B. R. Ramachandran, L. G. Gutsev, W.-J. Zheng, O. C. Thomas, and Kit H. Bowen


Articles you may be interested in

Benzene analogues of (quasi-)planar M@B n H n compounds (M = V−, Cr, Mn+): A theoretical investigation
J. Chem. Phys. 139, 174310 (2013); 10.1063/1.4827517

Electronic and geometrical structure of Mn 13 anions, cations, and neutrals
J. Chem. Phys. 129, 044310 (2008); 10.1063/1.2956494

Theoretical study of structure and photoelectron spectroscopy of In x P y − and In x P y (x + y 6) clusters
J. Chem. Phys. 124, 184316 (2006); 10.1063/1.2194553

Structural and electronic properties of Ge n m− and KGe n − Zintl anions (n=3–10;m=2–4) from density functional theory
J. Chem. Phys. 117, 606 (2002); 10.1063/1.1482068

Electronic structure of vanadium cluster anions as studied by photoelectron spectroscopy
J. Chem. Phys. 106, 2182 (1997); 10.1063/1.473785
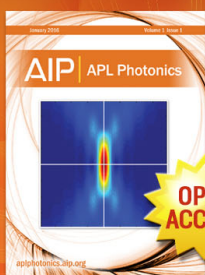
Photoelectron spectra and structure of the Mn$_n^-$ anions (n = 2–16)

G. L. Gutsev,[1,a)] C. A. Weatherford,[1] B. R. Ramachandran,[2] L. G. Gutsev,[3] W.-J. Zheng,[4]
O. C. Thomas,[4] and Kit H. Bowen[4,b)]

[1]*Department of Physics, Florida A&M University, Tallahassee, Florida 32307, USA*
[2]*College of Engineering and Science, Louisiana Tech University, Ruston, Louisiana 71272, USA*
[3]*Department of Chemistry and Biochemistry, Florida State University, Tallahassee, Florida 32306, USA*
[4]*Departments of Chemistry and Materials Science, Johns Hopkins University, Baltimore, Maryland 21218, USA*

Photoelectron spectra of the Mn$_n^-$ anion clusters (n = 2–16) are obtained by anion photoelectron spectroscopy. The electronic and geometrical structures of the anions are computed using density functional theory with generalized gradient approximation and a basis set of triple-ζ quality. The electronic and geometrical structures of the neutral Mn$_n$ clusters have also been computed to estimate the adiabatic electron affinities. The average absolute difference between the computed and experimental vertical detachment energies of an extra electron is about 0.2 eV. Beginning with n = 6, all lowest total energy states of the Mn$_n^-$ anions are ferrimagnetic with the spin multiplicities which do not exceed 8. The computed ionization energies of the neutral Mn$_n$ clusters are in good agreement with previously obtained experimental data. According to the results of our computations, the binding energies of Mn atoms are nearly independent on the cluster charge for n > 6 and possess prominent peaks at Mn$_{13}$ and Mn$_{13}^-$ in the neutral and anionic series, respectively. The density of states obtained from the results of our computations for the Mn$_n^-$ anion clusters show the metallic character of the anion electronic structures. © 2015 AIP Publishing LLC. [http://dx.doi.org/10.1063/1.4926943]

I. INTRODUCTION

A single Mn atom with the effective electron configuration of 3d^{5}4s^2 possesses a large total spin magnetic moment of 5 Bohr magnetons (μ_B); therefore, it might be anticipated that Mn$_n$ clusters possess larger total spin magnetic moments than corresponding Fe$_n$ clusters. However, this is true only for smaller Mn$_n$ clusters. A ferro- to ferri-magnetic transition occurs at n = 5 in the neutral clusters.[1,2] The transition was found to depend on the cluster charge, since the transition value of n changes[3–5] from 6 to 3 for Mn$_n^-$ and Mn$_n^+$, respectively. In order to stabilize ferromagnetic states of larger Mn$_n$ clusters, one can use their encapsulation inside shells composed of magnetic or nonmagnetic[6] atoms or doping them.[7]

The total spin magnetic moment of the gold-coated [Mn$_{13}$@Au$_{20}$] cluster is[8] 44 μ_B, whereas the total spin magnetic moment of free-standing Mn$_{13}$ is only 3 μ_B. However, the value of 44 μ_B still corresponds to a ferrimagnetic state of Mn$_{13}^-$ and its ferromagnetic state would have a total spin magnetic moment of ~65 (13 × 5) μ_B. Much higher total spin magnetic moments per atom can be obtained by using Mn as a coating material, e.g., in a Co$_{13}$@Mn$_{20}$ cluster whose total spin magnetic moment is 113 μ_B.[9] Since the total spin magnetic moment of free-standing Co$_{13}$ is 27 μ_B,[10] the Mn shell adds 86 μ_B, which is somewhat smaller than the sum of total spin magnetic moments of 20 free Mn atoms. Adding a single Mn

atom to a magnetic or nonmagnetic cluster results[11–16] in an increase of the total cluster spin magnetic moment by 3–5 μ_B, whereas adding a single 3d-metal atom[17] to Mn$_{12}$ or a nitrogen atom[18] to Mn$_n$ can increase their total spin magnetic moments by an order of magnitude.

Manganese is widely used for doping semiconductor quantum dots (QD). It was found[19,20] that Mn-doped QDs possess magnetic size-dependent properties similar to those of dilute magnetic semiconductors, which can be advantageous in spintronic applications.[21] Magnetic properties of Mn-doped CdSe QDs were probed by EPR over a wide range of QD diameters.[22,23] The EPR spectra of Mn-doped CdSe QDs with low concentrations of Mn contain sextet features which correspond to the total spin magnetic moment of 5 μ_B and oxidation state of +2 for the dopant atoms.

Homogeneous Mn clusters have received considerable attention from both experimentalists and theoreticians. On the experimental side, photoelectron spectra were obtained for Mn$_n^-$, n = 3–8,[24] and Mn$_{13}^-$,[25] whereas energies of electron detachment from neutral Mn$_n$ clusters have been measured[26] in the range 7 ≤ n ≤ 64. Stern-Gerlach experiments were performed for Mn$_n$ clusters in two ranges: 11 ≤ n ≤ 99[27] and 5 ≤ n ≤ 22.[28] The largest differences in total magnetic moments per atom for a Mn$_n$ with respect to its Mn$_{n-1}$ and Mn$_{n+1}$ neighbors were observed for n = 13 and 19. Optical spectra were obtained[29] for the Mn$_3^+$ trimer, and dissociation energies were measured[30,31] for Mn$_n^+$ in the range of 2 ≤ n ≤ 7.

Special attention was paid by theoreticians to the neutral Mn$_{13}$ cluster which was found[32–38] to possess a slightly distorted icosahedral geometrical structure and a total spin magnetic moment of 3 μ_B. Smaller neutral Mn$_n$ have also been

---

a)Author to whom correspondence should be addressed. Electronic mail: gennady.gutsev@famu.edu
b)Author to whom correspondence should be addressed. Electronic mail: kbowen@jhu.edu

    143, 044306-1

the subject of a number of studies.[39–42] Bobadova-Parvanova *et al.*[43] and Kabir *et al.*[44] have considered the Mn_n series in the ranges of $2 \leq n \leq 13$ and $2 \leq n \leq 20$, respectively. Non-collinear magnetic effects were studied[45–47] for small Mn_n clusters ($n = 2$–7) using density functional theory within both Local-Spin Density Approximation (LSDA) and generalized gradient approximation (GGA). The states of Mn_n clusters with a noncollinear ordering of local total spin magnetic moments appear at $n > 6$ and such states are marginally below the states with a collinear ordering in total energy. The largest collinear-noncollinear difference of 0.18 eV was found for the Mn_9 cluster,[48] whereas the lowest total energy states of larger Mn_n clusters with $n = 13$, 15, and 19 are found to be collinear.

This work is aimed at a systematic study of the electronic structure of the Mn_n^- cluster anions in the range of $2 \leq n \leq 16$. Experimental data have been obtained using laser anion photoelectron spectroscopy and their interpretation was based on the results of our density functional theory computations. We also optimized both neutral Mn_n clusters in order to evaluate the adiabatic electron affinities and singly positively charged Mn_n^+ clusters in order to compare ionization energies of the neutrals with previous experimental data. We also plotted theoretical total densities of states for some selected Mn_n^- clusters using the results of computations for the corresponding lowest total energy states and compared them with the experimental spectra of these clusters.

II. EXPERIMENTAL METHODS

A. Photoelectron spectra of Mn_n^-

Anion photoelectron spectroscopy is conducted by crossing a mass-selected beam of negative ions with a fixed-frequency photon beam and energy-analyzing the resultant photoelectrons. It is governed by the energy-conserving relationship, $h\nu = E_{BE} + E_{KE}$, where $h\nu$ is the photon energy, E_{BE} is the electron binding (transition) energy, and E_{KE} is the electron kinetic energy.

Manganese cluster anions, Mn_n^-, were produced and characterized on our pulsed photoelectron instrument. They were generated in a laser vaporization ion source by focusing a pulsed (10 Hz), second harmonic (532 nm) beam of a Nd:YAG laser onto a continuously rotating, translating manganese rod. Ultra-high purity He carrier gas was used in the pulsed valve with a backing pressure of ~150 psi. The resultant anions were then extracted into a linear time-of-flight mass spectrometer, mass-selected by a mass gate, decelerated by a momentum decelerator, and photodetached by a Nd:YAG laser operated at the third harmonic (355 nm, 3.49 eV). The resultant photoelectrons were analyzed by a magnetic bottle electron energy analyzer with a resolution of 35 meV at $E_{KE} = 1$ eV. The photoelectron spectra were calibrated against the well-known photoelectron spectrum of Cu^-.

III. CALIBRATION OF COMPUTATIONAL METHODS

In order to gain insight into the dependence of computational results on the basis and method used, we performed calibration calculations for the Mn_2^- anion. Assignment of the

ground state of neutral Mn_2 dimer is challenging and is still under debate. The lowest total energy state of the dimer was found to possess the spin multiplicity of 11 if computed using density functional theory methods,[49–51] whereas Hartree-Fock based studies[52–57] have predicted a singlet $^1\Sigma_g^+$ state to be the ground state of Mn_2. The latter is in agreement with an early experimental ESR study which predicted a singlet antiferromagnetic state for the dimer.[58]

Detachment of an electron from Mn_2^- results in the formation of the $^{12}\Sigma_g^+$ ground state of the Mn_2^+ cation.[59] No experimental data are available on the nature of the Mn_2^- anion; therefore, we tested its states with $2S + 1 = 2$ and 10, which are found to have the lowest total energies among ferrimagnetic and ferromagnetic states, respectively. We optimized the Mn–Mn bond length and computed vertical electron detachment energies (VDEs) of both states using 10 methods and the 6-311+$G(3df)$ basis set.[60] Computations on the ferrimagnetic $2S + 1 = 2$ state have been performed with broken symmetry.

Within our selection, density functional theory (DFT) is presented by the BPW91,[61,62] PW91,[63] BLYP,[64] and PBE[65] methods with GGAs to the exchange-correlation functional along with the PZKB[66] and TPSS[67] methods with the τ-dependent gradient-corrected exchange-correlation functionals. The hybrid Hartree-Fock-DFT group is presented by the B3LYP[68] and B3PW91 methods, whereas long-range corrected methods are presented by the CAM-B3LYP[69] and ωB97XG[70] methods. All our computations are performed using the GAUSSIAN 09 suite of programs.[71]

The results of computations are presented in Table I. As can be seen, all methods predict the high-spin state to have the lowest total energy, except for the CAM-B3LYP method which predicts a $^{10}\Sigma_g^-$ state to be unstable with

TABLE I. Vertical detachment energies (VDE) for two states of the Mn_2^- anion and the difference in total energies of the states.[a]

Initial state of Mn_2^-	$^{10}\Sigma_g^-$		$2S + 1 = 2$		
Final state of Mn_2	$^9\Sigma_u^-$	$^{11}\Pi_u$	$2S + 1 = 1$	$2S + 1 = 3$	ΔE_{tot}[b]
Method			Ionization energy		
Semilocal DFT					
BPW91	1.21	**0.74**	0.95	1.04	0.31
PW91	1.69	**0.82**	0.88	1.22	0.32
PBE	1.20	**0.78**	0.64	1.21	0.33
BLYP	1.46	**0.79**	0.74	1.22	0.27
TPSS	1.20	**0.67**	0.91	1.11	0.32
PKZB	1.64	**0.50**	0.68	1.21	0.32
Hybrid DFT					
B3LYP	1.60	**0.89**	0.56	1.46	0.20
B3PW91	1.71	**0.82**	0.50	1.51	0.20
CAM- B3LYP	Unbound		**0.34**	1.63	…
ωB97XD	1.65	**1.06**	0.43	1.49	0.19
Experiment			0.38 ± 0.08[c]		

[a]All values are in eV, the smallest values to be compared to the experimental value are given in bold.
[b]The difference in total energy of two anion states $\Delta E_{tot} = E_{tot}(2S + 1 = 2) - E_{tot}(^{10}\Sigma_g^-)$.
[c]This work.

TABLE II. Comparison of vertical detachment energies of an extra electron computed using different methods and basis sets with experiment for Mn_n^- (n = 3–7).[a]

Method	Basis \ 2S + 1	Mn_3^- 15	Mn_4^- 20	Mn_5^- 23	Mn_6^- 8	Mn_7^- 3
BPW91	6-311+G*	1.33	1.70	1.54	1.46	1.49
	6-311+G(3df)	1.33	1.72	1.56	1.46	1.49
	cc-pVTZ	1.29	1.69	1.52	1.45	1.47
PKZB	6-311+G*	1.19	1.48	1.29	1.23	1.44
	6-311+G(3df)	1.19	1.54	1.31	1.23	1.43
	cc-pVTZ	1.14	1.47	1.26	1.20	1.55
TPSS	6-311+G*	1.26	1.60	1.48	1.34	1.44
	6-311+G(3df)	1.27	1.63	1.51	1.34	1.46
	cc-pVTZ	1.22	1.60	1.46	1.32	1.41
Expt.[b]		1.13 ± 0.08	1.49 ± 0.08	1.48 ± 0.08	1.73 ± 0.08	1.75 ± 0.08

[a] All values are in eV, the smallest values to be compared to the experimental value are given in bold.
[b] This work.

respect to dissociation. The VDEs corresponding to the $^{10}\Sigma_g^- \rightarrow {}^{11}\Pi_u$ (neutral ground state) are to be compared to the experimental value of 0.38 ± 0.08 eV. The closest value is provided by the PKZB method, where the difference from the experimental value when taking into account the uncertainty bars is 0.04 eV. Among the GGA-DFT methods, the lowest value of 0.74 eV obtained at the BPW91 level of theory is above the experimental top boundary value by +0.27 eV. The TPSS value is between the BPW91 and PKZB values, whereas the values obtained using HF-DFT methods are larger than the BPW91 value. Therefore, we choose the BPW91, TPSS, and PKZB methods for further testing on Mn_n^- in the range of $3 \leq n \leq 7$.

Table II presents the results of computations using these three methods and three basis sets: 6-311+G*, 6-311+G(3df), and cc-pVTZ[72] which contains much more primitives than Pople's basis sets. The geometries were optimized at each method-basis combination followed by the VDE calculations. If the initial state of an anion is not a singlet and has the spin multiplicity of M, then the final neutral states have the spin multiplicities of M ± 1, where the sign depends on which spin representation the ejected electron belonged to. The computed VDEs presented in Table II correspond to the smallest VDE value obtained for a given anion. As can be seen, the dependence on the basis set is quite small especially in the BPW91 case. The BPW91/6-311+G* values are within 0.01-0.04 eV of the values obtained using the cc-pVTZ basis set. The PKZB values are closer to the experimental values for Mn_3^-, Mn_4^-, and Mn_7^-, but significantly smaller than the experimental values for Mn_6^-. On the whole, the BPW91 method appears to be more consistent than the other two methods. Therefore, the rest of our computations was performed using the BPW91/6-311+G* approach. It is worth noting that the BPW91 method was found to be more stable in harmonic vibrational frequency computations[73] than some other density functional theory with generalized gradient approximation (DFT-GGA) methods.

For each Mn_n^- anion, we performed a search of its optimal geometric structure and total spin using a number of guess structures obtained in previous computations on Mn_n

and its ions. For n = 14–16, we used additional geometrical structures obtained in our previous work on Fe_n and Fe_n^- clusters.[74] Geometrical structures found for a couple of lowest total energy states of a given anion have been used as initial geometries in optimizations of the corresponding neutrals and cations. A search for the lowest total energy ferrimagnetic state is rather complicated, because there are a large number of possible orientations of the local total spin magnetic moments. For example, the number of possible spin-up and spin-down distributions of the local spin magnetic moments in an antiferromagnetic singlet of Mn_{16} is C(16, 8) = 12 870.

When searching for the lowest total energy states we used spin-up and spin-down combinations produced in computations on singly and doubly charged ferrimagnetic states of a given species. In addition, we moved back and forth in the spin multiplicity using previously optimized states with smaller or larger spin multiplicities as guesses. Each geometry optimization was followed by an analytical second derivatives calculation of the harmonic vibrational frequencies in order to confirm that the optimized geometry corresponds to a minimum. The convergence threshold for total energy was set to 10^{-8} eV and the force threshold was set to 10^{-3} eV/Å. Local total spin magnetic moments on atoms were obtained using natural atomic orbital (NAO) populations computed using the Natural Bond Orbital (NBO) suite.[75]

IV. RESULTS AND DISCUSSION

Figure 1 presents a mass spectrum of the Mn_n^- cluster anions generated in this study and Figure 2 shows the anion photoelectron spectra of Mn_n^-, n = 2–16 measured in this work. These photoelectron spectra show photodetachment transitions from the ground state of each of these mass-selected manganese cluster anions to the ground and excited vibronic states of their corresponding neutral clusters. The lowest electron binding energy (E_{BE}) peak/band in each spectrum reflects a transition from the anion ground state to the neutral ground state, and as such it provides the electron affinity for that particular manganese cluster size. Higher E_{BE}
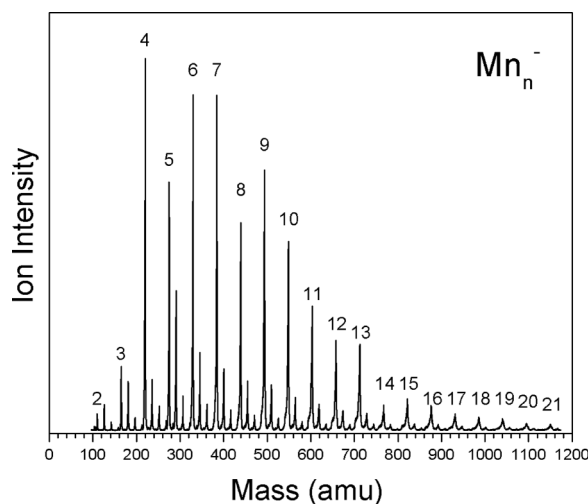
FIG. 1. A mass spectrum of the manganese cluster anions, Mn_n^-.

FIG. 2. The anion photoelectron spectra of the mass-selected manganese cluster anions, Mn_n^-, $n = 2$–16. These spectra were all measured with 355 nm photons.

peaks reflect transitions from a given ground state Mn_n^- cluster anion to various excited electronic/vibronic states of the corresponding neutral Mn_n clusters. All of these transitions are vertical in that they access the neutral (final) states at the geometry of the anion from which they came.

We will first discuss the geometrical structures and spin magnetic moments of the lowest total energy states in the Mn_n^- and Mn_n series. Next, we will compare the results of our computations on the electron affinities and ionization energies to the experimental data. The total density of states (DOS) computed for several Mn_n^- anions will be compared to the corresponding electron photodetachment spectra. Finally, we consider binding energies in the neutral and anionic series.

A. Geometrical configurations and magnetic moments

The geometrical structures and total spins of Mn clusters in the range of $2 \leq n \leq 6$ presented in Figure 3 are similar to those found previously, except for Mn_6 where different local total spin magnetic moments are obtained in the lowest total energy state with the spin multiplicity of 9. The distribution of the local spin magnetic moments in Figure 3 is the same as obtained by Bobadova-Parvanova *et al.*[43] In addition to the previous results, we performed optimizations within actual symmetry constraints of the clusters and have obtained spectroscopic states in both neutral and anionic series. Optimizations of larger clusters have been performed without symmetry constraints.

Figure 4 presents the geometrical structures obtained for the lowest total states of the Mn_n^- and Mn_n clusters in the range of $7 \leq n \leq 11$. The cluster growth proceeds by adding Mn atoms to the pentagonal bipyramid structure of Mn_7. During the growth, atoms with spin-down local total spin magnetic moments are arranged in such a way as to form an octahedron in both Mn_{11} and Mn_{11}^-. The spin multiplicities of the neutral and its anion differ by one in all pairs except for $n = 7$, where the difference is 3. Comparison of the corresponding bond lengths between an anion and its
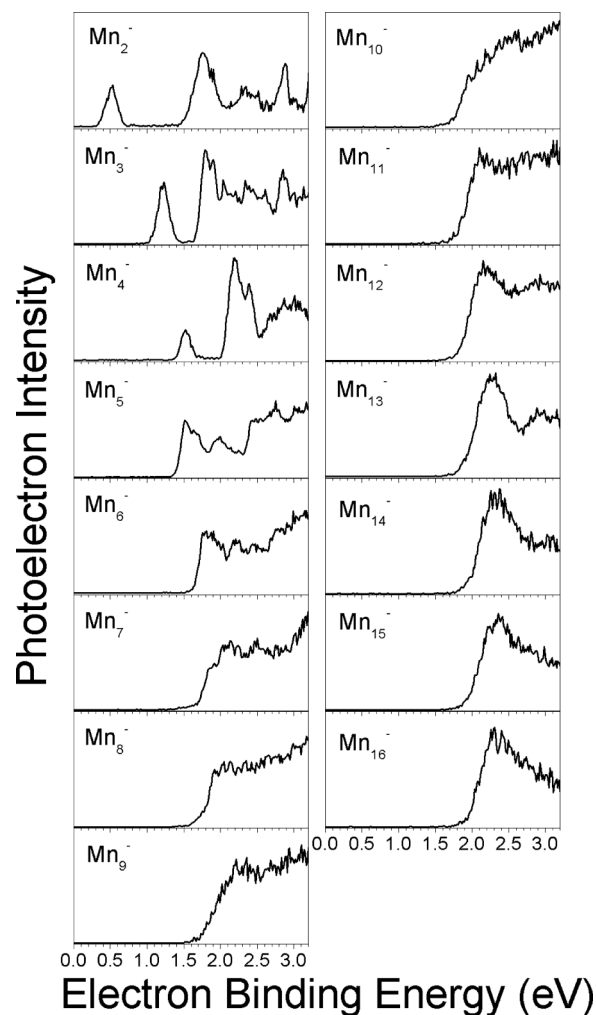
neutral parent generally shows small relaxations in the bond lengths. The anion bond lengths are sometimes shorter than the corresponding bond lengths of the neutral as can be seen from comparison of bond lengths in Mn_{11} and Mn_{11}^-.

The geometrical structures of Mn_{12} and Mn_{12}^- possess different topologies and the difference in their spin multiplicities is 3 (see Figure 5) and atoms with spin-down total magnetic moments form octahedrons. Both Mn_{13} and Mn_{13}^- possess distorted I_h geometrical structures with similar distributions of local total spin magnetic moments obtained in the previous work. Similar to the Fe_{14}–Fe_{14}^- pair, the geometrical structures of the Mn_{14}–Mn_{14}^- pair are formed by adding a Mn atom to a top triangle of an icosahedron. When adding one more Mn atom, a serious reconstruction of Mn_{14}^- is observed. Almost all Mn_n and Mn_n^- possess a number of isomers which are within 0.1–0.3 eV of the total energy of the ground state. The Mn_{15}–Mn_{15}^- pair present a special case where the states with the spin multiplicities of 6 (Mn_{15}) and 5 (Mn_{15}^-) are practically degenerate in total energy with the states with the spin multiplicities of 28 (Mn_{15}) and 27 (Mn_{15}^-). The dependence of geometrical shape on the spin multiplicity is shown in Figure 6 for the Mn_{16}–Mn_{16}^- pair. As can be
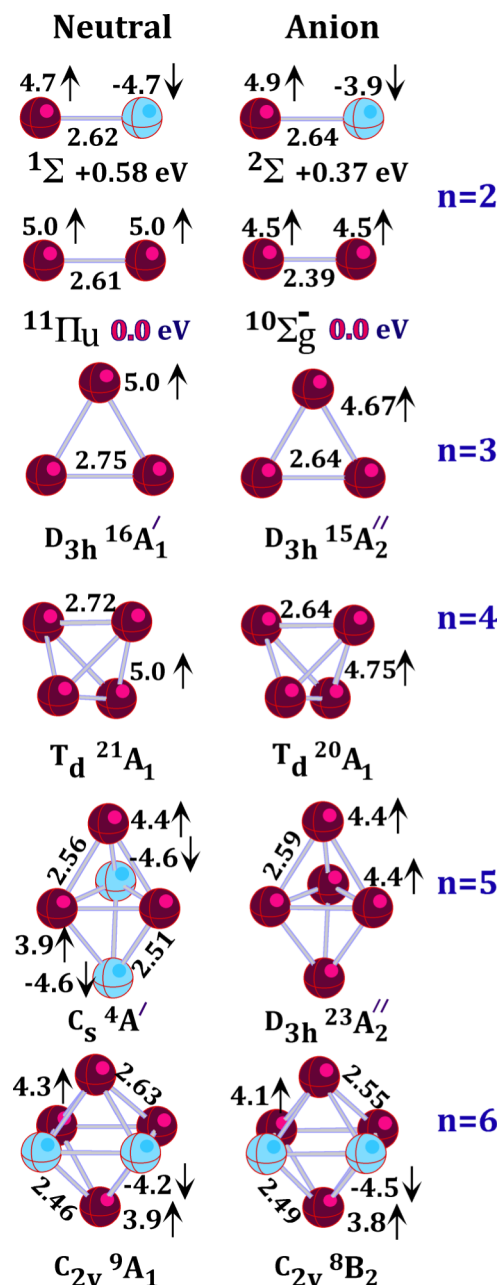
FIG. 3. Geometrical structures and local spin magnetic moments for the lowest total energy states of the neutral and charged Mn$_n$ clusters, $n = 2$–6. Bond lengths are in ångströms and local spin magnetic moments are in Bohr magnetons.
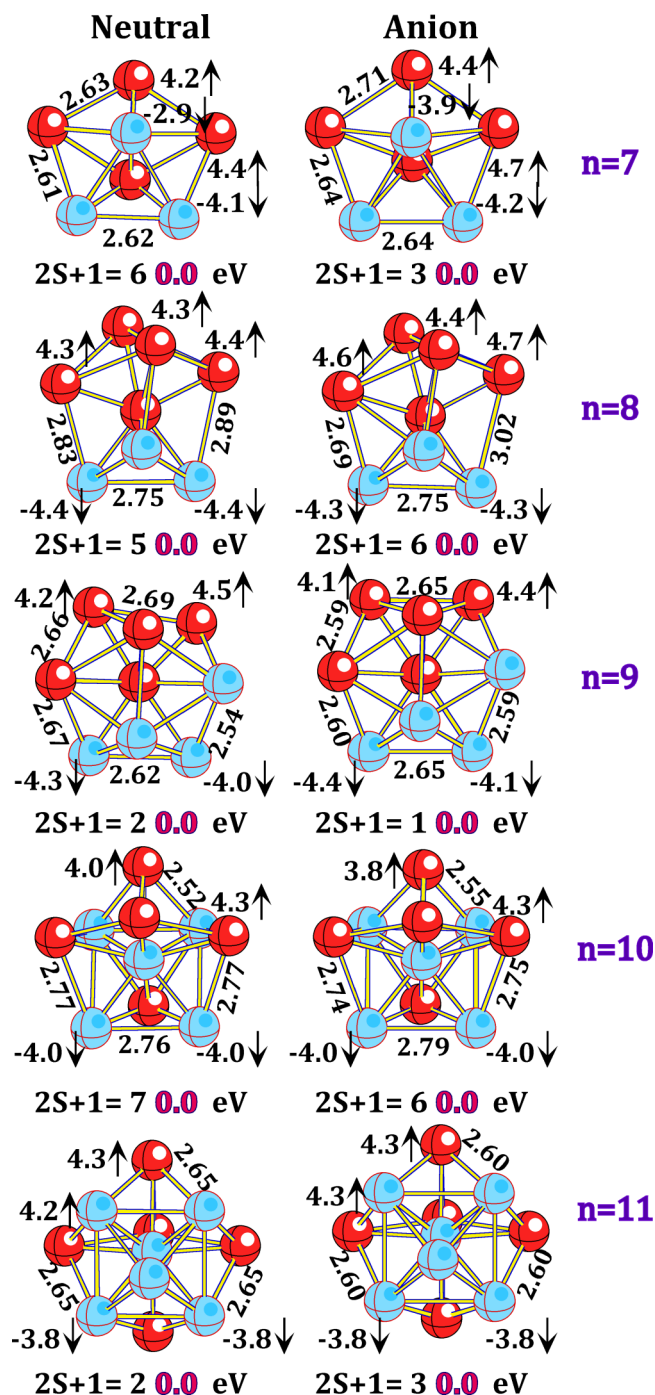

FIG. 4. Geometrical structures and local spin magnetic moments for the lowest total energy states of the neutral and charged Mn$_n$ clusters, $n = 7$–11. Bond lengths are in ångströms and local spin magnetic moments are in Bohr magnetons.

seen in the figure, the geometrical shape can be significantly modified by changes in the spin multiplicity or charge. In addition, a state with a different geometrical topology may have a lower total energy than states with geometrical structures derived from the geometry of the lowest total energy states.

A survey of Figures 3–6 shows that the local total spin magnetic moments on the atoms are around 4 μ_B. The moments are mainly due to the difference in the populations of 3d atomic orbitals of a given atom. Since the α-3d subshell is occupied by 5 electrons, this means that the β-3d subshell is occupied by a single electron. Occupations of 4s and 4p AOs of a given atom are approximately equal and do not contribute to the

local total spin magnetic moment. However, only surface Mn atoms possess high total spin magnetic moments. If a Mn atom is inside the cage formed by other Mn atoms (e.g., the central atom in Mn$_{13}$), then its total spin magnetic moment sharply decreases and all 3d electrons can participate in the bonding with surface atoms.

The spin multiplicities of the lowest total energy states of Mn$_n$ clusters for $n = 3$–7 and 13 obtained in the present and previous work are the same, but it is not so for the clusters with other n values. Comparison of the spin multiplicities
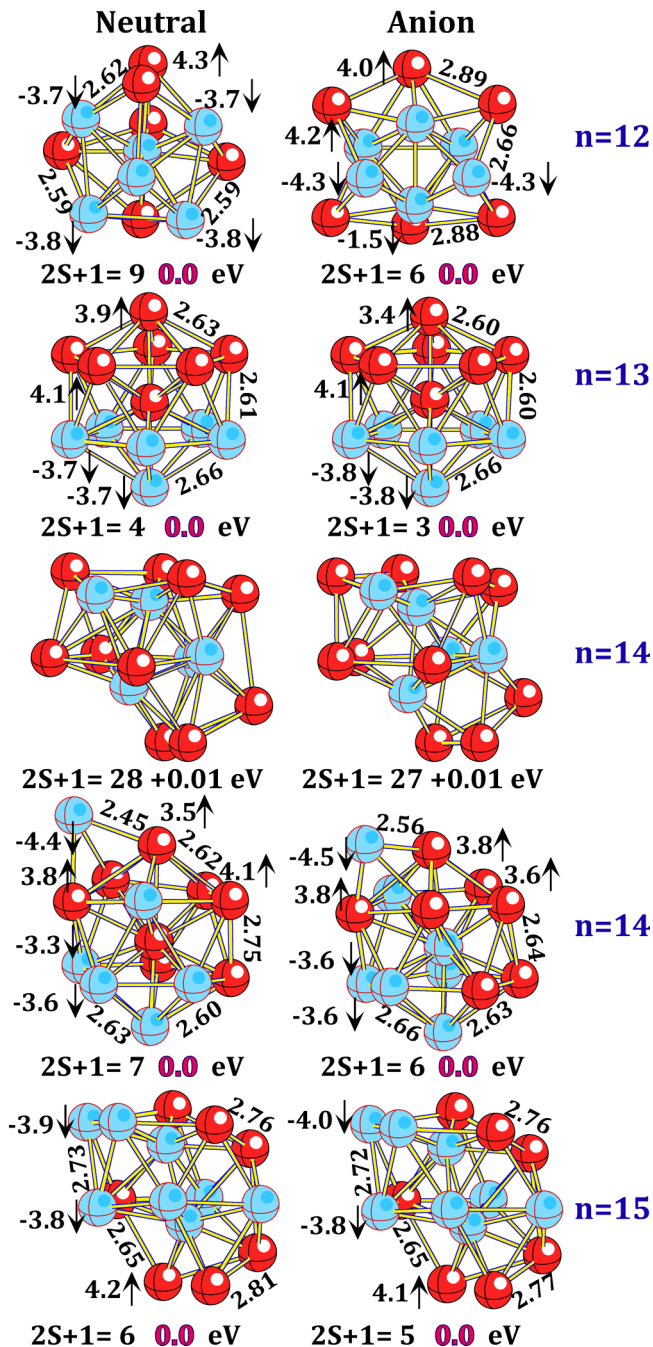
FIG. 5. Geometrical structures and local spin magnetic moments for the lowest total energy states of the neutral and charged Mn$_n$ clusters, n = 12–15 along with the geometrical structures of the states next to the lowest total energy states of Mn$_{15}$ and Mn$_{15}^-$.

FIG. 6. Geometrical structures and local spin magnetic moments for the lowest total energy states of the neutral and charged Mn$_{16}$ clusters along with the geometrical structures of three excited states.

obtained in this work with the spin multiplicities obtained by Kabir *et al.*[44] using a pseudopotential plane wave method is presented in Figure 7. As can be seen from Kabir *et al.*[44] (a) and our (b) curves, our all-electron approach predicts smaller spin multiplicity values in the range of $8 \leq n \leq 16$ except for n = 13. Experimental values of the total magnetic moment $\mu = (2S + L)$, where L and S are the total angular and spin moments, respectively, measured[27] for Mn$_n$ clusters are generally larger than the total spin magnetic moments obtained from the present computations. Contributions of the orbital moments to the total magnetic moments have experimentally
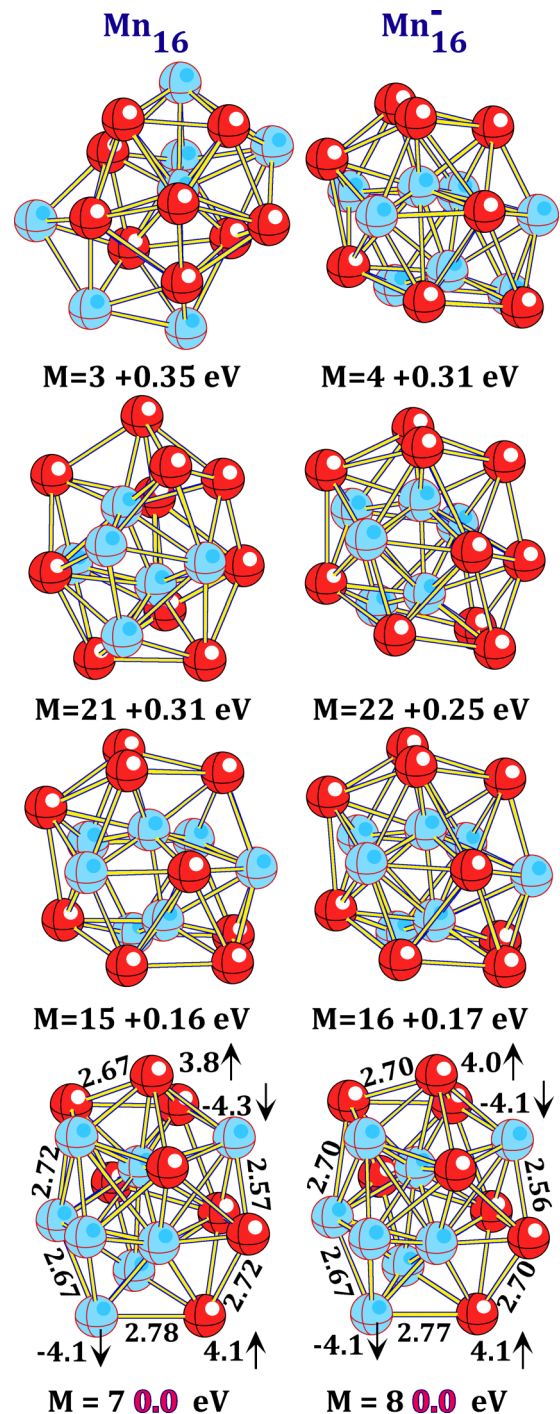
been measured for the Fe$_n$, Co$_n$, and Ni$_n$ clusters and found to be quite significant.[76–78] Therefore, our computed total spin magnetic moments ought to be smaller than the experimental values obtained for the total magnetic moments.

B. Electron affinity and vertical electron detachment energies

Laser detachment of an electron from an anion corresponds to an instant event when the geometry of a neutral
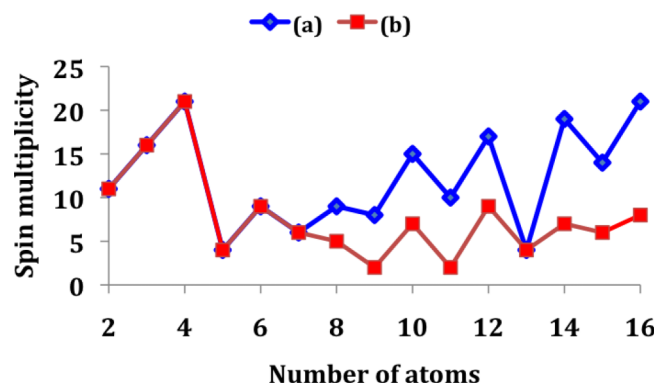
FIG. 7. Spin multiplicities of the lowest total energy states of the neutral Mn_n clusters: (a) from Ref. 44 and (b) this work.

produced is unrelaxed (a so-called vertical detachment of an electron). Theoretically, the electron detachment energy can be computed as the difference in total electronic energies of the anion and the neutral formed at the equilibrium anion geometry according to the equation,

$$E_{VDE}(Mn_n^-) = E_{tot}^{el}(Mn_n, R_e^-) - E_{tot}^{el}(Mn_n^-, R_e^-), \quad (1)$$

where R_e^- denotes the anion equilibrium geometry. If the anion spin multiplicity $2S + 1 > 1$, then the final neutral states may have the spin multiplicity of $2S$ or $2S + 2$. On the contrary, the adiabatic electron affinity (EA_{ad}) corresponds to the energy gained due to the attachment of an extra electron. The EA_{ad} of a neutral species can be computed as the difference in total energies of the lowest total energy states of an anion and its neutral parent,

$$EA_{ad}(Mn_n) = [E_{tot}^{el}(Mn_n) + E_0(Mn_n)]$$
$$- [E_{tot}^{el}(Mn_n^-) + E_0(Mn_n^-)], \quad (2)$$

where E_{tot}^{el} is the total Born-Oppenheimer energy and E_0 is the zero-point vibrational energy.

Our EA_{ad} and VDE values for the Mn_n and Mn_n^-, respectively, computed in the whole range of $2 \leq n \leq 16$ are presented in Table III. Comparison of the EA_{ad} and VDE values shows that adiabatic relaxation can be quite large in the beginning of the series (0.37 eV for $n = 6$) and is close to 0.1 eV by the end of the series. The smallest of the two computed VDE values for each species has to be compared to the experimental values displayed in the last column. Comparison shows the largest difference between theoretical and experimental data to be -0.26 eV with respect to the experimental lowest boundary value for $n = 8$. At larger n, the difference is smaller and does not exceed 0.1 eV.

Amazingly, the vertical detachment energies are nearly independent of the spin multiplicity for larger clusters as shown in Figure 8 for Mn_{16}^-. As can be seen, total energy (curve (a)) depends on the spin multiplicity and appreciably rises at $2S + 1 > 24$. However, the VDE energies are all around the experimental value of 2 eV within the experimental uncertainty bars of ±0.08 eV for both $2S$ and $2S + 2$ final states (curves (b) and (c), respectively).

Figure 9 presents the computed adiabatic electron affinities as curve (a). The curve shows quite a monotonous character with a slow rise toward larger n values. We have also computed energies of adiabatic electron detachment from the neutral Mn_n clusters as the differences in total energy of the lowest total energy states of Mn_n and Mn_n^+. Our computed adiabatic ionization energies are presented in Figure 9 together with experimental values[26] obtained for the neutral manganese clusters for $n > 6$ within the uncertainty bars of ±0.05 eV (curves (b) and (c), respectively). Theoretical and experimental values are practically the same within the experimental uncertainty bars, which can be considered

TABLE III. Comparison of vertical detachment energies from the lowest total energy states of the M_n^- anions computed at the BPW91/6-311+G* level with experiment.[a]

		Vertical electron detachment energies			
n	Adiabatic electron affinity[b]	Initial anion state $2S+1$	Final neutral state $2S$	Final neutral state $2S+2$	Experiment[c]
2	0.58	10	1.21	**0.73**	0.48 ± 0.08
3	1.27	15	1.75	**1.33**	1.13 ± 0.08
4	1.64	20	2.07	**1.70**	1.49 ± 0.08
5	1.36	23	1.92	**1.54**	1.48 ± 0.08
6	1.41	8	1.77	**1.46**	1.73 ± 0.08
7	1.39	3	**1.49**	1.68	1.75 ± 0.08
8	1.34	6	**1.41**	1.71	1.75 ± 0.08
9	1.49	1	...	1.57	1.80 ± 0.08
10	1.68	6	1.83	**1.75**	1.85 ± 0.08
11	1.54	3	**1.61**	1.74	1.90 ± 0.08
12	1.66	6	**1.92**	1.97	1.90 ± 0.08
13	1.84	3	2.12	**1.92**	1.90 ± 0.08
14	1.93	6	2.01	**2.01**	1.95 ± 0.08
15	1.88	5	1.98	**1.93**	1.98 ± 0.08
16	1.94	8	**2.00**	2.07	2.00 ± 0.08

[a]All values are in eV, the smallest values to be compared to the experimental value are given in bold.
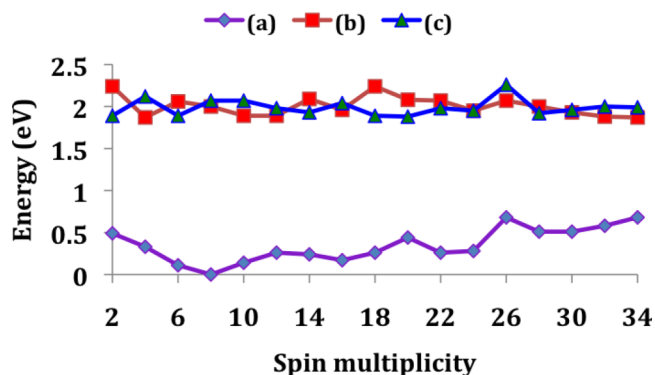[b]Computational results of this work.
[c]This work.

FIG. 8. Total energies relative to that of the $2S+1=8$ state and vertical electron detachment energies of Mn_{16}^{-} as a function of spin multiplicity: (a) total energies, (b) final neutral states with the spin multiplicity of $2S$; (c) final neutral states with the spin multiplicity of $2S+2$.

as confirmation of the reliability of the BPW91/6-311+G* approach used.

C. Binding energies

In order to gain insight into thermodynamic stability of Mn_n and Mn_n^{-}, we have computed the energies of a Mn atom abstraction in the neutral and anionic series. The binding energies of Mn_n and Mn_n^{-} have been computed according to the equations,

$$E_b(Mn_n) = E_{tot}^{el}(Mn_{n-1}) + E_0(Mn_{n-1}) + E_{tot}^{el}(Mn) \\ - [E_{tot}^{el}(Mn_n) + E_0(Mn_n)], \quad (3)$$

$$E_b(Mn_n^{-}) = E_{tot}^{el}(Mn_{n-1}^{-}) + E_0(Mn_{n-1}^{-}) + E_{tot}^{el}(Mn) \\ - [E_{tot}^{el}(Mn_n^{-}) + E_0(Mn_n^{-})], \quad (4)$$

where E_{tot}^{el} is the total Born-Oppenheimer energy and E_0 is the zero-point vibrational energy. Note that the Mn atom cannot form an anion[79] which results in an interesting relationship between binding energies of the neutral and anionic clusters. Subtracting Eq. (4) from (3), one obtains

$$E_b(Mn_n) - E_b(Mn_n^{-}) = EA_{ad}(Mn_{n-1}) - EA_{ad}(Mn_n). \quad (5)$$

This relationship is reflected in Figure 10, where the neutral (a) and anionic (b) binding energies are close to each other if there
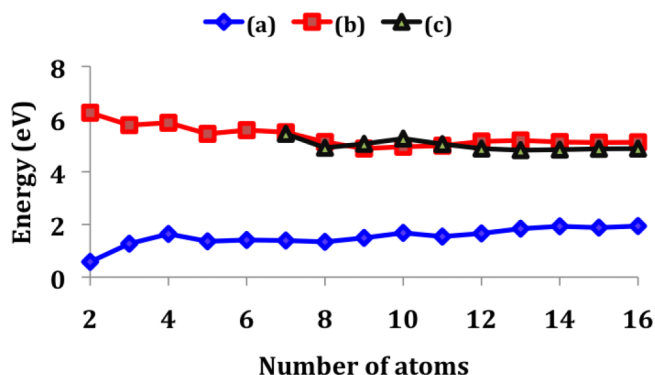

FIG. 9. Neutral Mn_n clusters: (a) computed adiabatic electron affinity, (b) computed ionization energies, (c) experimental ionization energies are from Ref. 26.
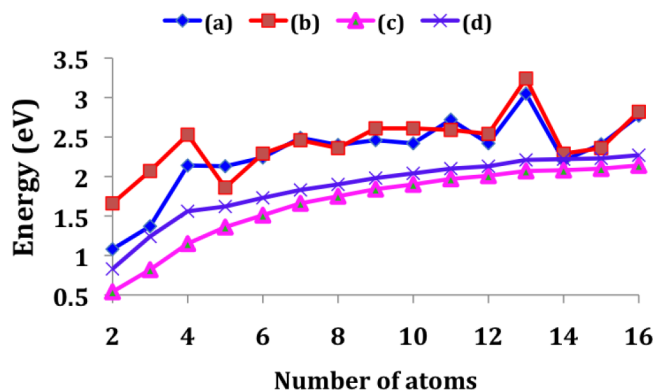

FIG. 10. Neutral Mn_n clusters: (a) energies of a single Mn atom abstraction, (c) atomization energies. Singly negatively charged Mn_n^{-} clusters: (b) energies of a single Mn atom abstraction, (d) atomization energies.

is no jump in the EA_{ad} consecutive values. On the whole, the anions are more stable than the corresponding neutrals except for n values of 5 and 11. A higher stability of the anions can also be confirmed by the results of computations on the atomization energies performed according to

$$E_{atom}(Mn_k^{0,-}) = [k E_{tot}^{el}(Mn) - \{E_{tot}^{el}(Mn_k^{0,-}) + E_0(Mn_k^{0,-})\}]/k \\ = \Sigma_{i=1}^{i=k} E_b(Mn_i), \quad (6)$$

where the binding energy of a single Mn atom in the right hand side summation is assumed to be zero. The anion atomization curve (d) is somewhat above the neutral atomization curve (c), which confirms a slightly higher stability of the anions on average.

D. Density of states

Total and partial DOS computed for the lowest total energy states of the Mn_n^{-} clusters for selected values of $n = 2, 4, 6, 8, 10, 14$, and 16 along with the DOS of an isomer of Mn_{16}^{-} are presented in Figure 11. One can see that contributions of the spin-up (or α) and spin-down (or β) constituents for larger clusters are of about same magnitude, which can be related to the ferrimagnetic nature of the corresponding electronic states. The Fermi level shifts to smaller energies as n increases and there is no gap in the DOS. The latter reflects a metallic character of the electronic structure in the Mn_n^{-} clusters. The total density of states can be compared[80] to the experimental spectra in Figure 2. As can be seen, there is a general resemblance between a total DOS and the corresponding photoelectron spectrum.

V. SUMMARY

This work presents a combined study of the Mn_n^{-} anion clusters in the range of n from 2 to 16 by experimental and theoretical methods. On the experimental side, we used anion photoelectron spectroscopy and DFT-GGA on the theoretical side. For each anion and its neutral parent, we explored a number of possible geometrical structures and spin configurations. The neutral and singly negatively charged Mn_n clusters have been previously studied using different
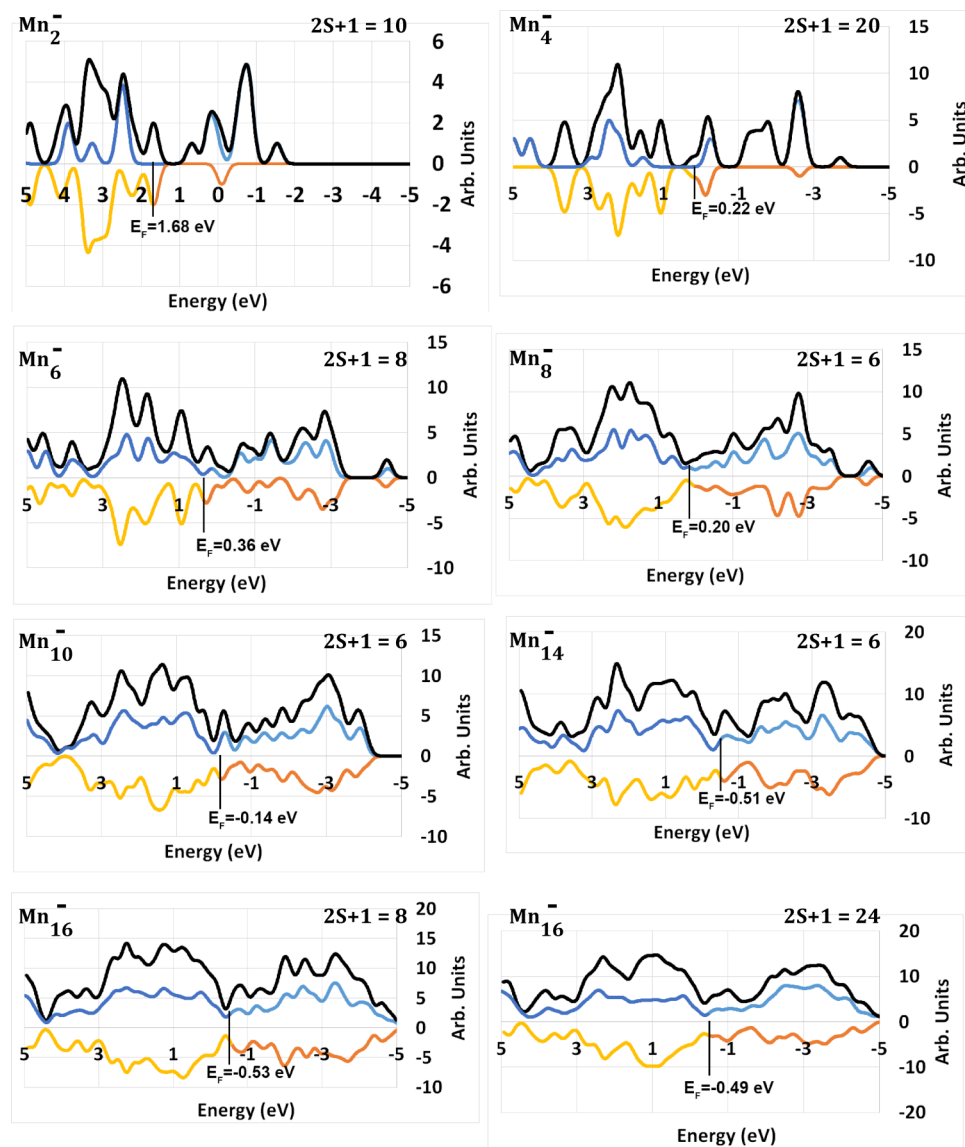
FIG. 11. Total density of states and their decomposition into α- and β-constituents (blue and yellow color, respectively) for the lowest total energy states of the Mn_2^-, Mn_4^-, Mn_6^-, Mn_8^-, Mn_{10}^-, Mn_{14}^-, and Mn_{16}^- clusters along with a Mn_{16}^- isomer.

methods for selected n values, whereas a systematic study of the Mn_n^- series in the whole range of $2 \leq n \leq 16$ is reported for the first time. In order to choose a method of calculations, we tested 10 methods with semilocal and hybrid exchange-correlation functionals on Mn_2^- and chose three methods: BPW91, PKZB, and TPSS, then we performed further testing on the Mn_n^- clusters with $n = 3$–7 using three basis sets: 6-311+G^*, 6-311+$G(3df)$, and cc-PVTZ. Based on the results of these test computations, the BPW91/6-311+G^* approach has been used for the manganese clusters with $n > 7$.

The Mn_n^- anion clusters possess a number of isomers with different geometrical structures and a large number of different local spin couplings at a given spin multiplicity $2S + 1$ for each state with a particular geometrical structure. Therefore, one needs a target which has to be reached while searching for the lowest total energy state. The anion photoelectron spectroscopy proved to be very useful in our search for these states. For smaller n values, the computed vertical ionization energies from the lowest total energy of the Mn_n^- anion clusters differ from the corresponding experimental values by less than 0.26 eV within the experimental uncertainty bars of

±0.08 eV. As n increases, both computed and experimental values nearly match each other. Therefore, one can anticipate that the anion states found in the present work are close to the states corresponding to the global minima.

ACKNOWLEDGMENTS

[1]P. Bobadova-Parvanova, K. A. Jackson, S. Srinivas, and M. Horoi, "Emergence of antiferromagnetic ordering in Mn clusters," Phys. Rev. A **67**, 061202(R) (2003).

[2]M. R. Pederson, F. Reuse, and S. N. Khanna, "Magnetic transition in Mn$_n$ (n = 2-8) clusters," Phys. Rev. B **58**, 5632–5636 (1998).

[3]S. K. Nayak, B. K. Rao, and P. Jena, "Equilibrium geometries, electronic structure and magnetic properties of small manganese clusters," J. Phys.: Condens. Matter **10**, 10863–10877 (1998).

[4]S. N. Khanna, B. K. Rao, P. Jena, and M. Knickelbein, "Ferrimagnetism in Mn$_7$ cluster," Chem. Phys. Lett. **378**, 374–379 (2003).

[5]G. L. Gutsev, M. D. Mochena, and C. W. Bauschlicher, Jr., "Structure and properties of Mn$_n$, Mn$_n^-$, and Mn$_n^+$ clusters (n = 3–10)," J. Phys. Chem. A **110**, 9758–9766 (2006).

[6]M. Wu and P. Jena, "Magnetic hollow cages with colossal moments," J. Chem. Phys. **139**, 044301 (2013).

[7]M. Wu and P. Jena, "Giant magnetic moments of B and C doped cuboctahedral Mn$_{13}$ clusters," Nanoscale **5**, 2114–2117 (2013).

[8]J. Wang, J. Bai, J. Jellinek, and X. C. Zeng, "Gold-coated transition-metal anion [Mn$_{13}$@Au$_{20}$]$^-$ with ultrahigh magnetic moment," J. Am. Chem. Soc. **129**, 4110–4111 (2007).

[9]Q. Jing, H.-B. Cao, G.-X. Ge, Y. Xuwang, H.-X. Yan, Z.-Y. Zhang, and Y.-H. Liu, "Giant magnetic moment of the core–shell Co$_{13}$@Mn$_{20}$ clusters: First-principles calculations," J. Comput. Chem. **32**, 2474–2478 (2011).

[10]G. L. Gutsev, L. E. Johnson, K. G. Belay, C. A. Weatherford, L. G. Gutsev, and B. R. Ramachandran, "Structure and magnetic properties of Fe$_{12}$X clusters," Chem. Phys. **430**, 62–68 (2014).

[11]N. Shen, J. Wang, and L. Zhu, "*Ab initio* study of magnetic properties of bimetallic Co$_{n-1}$Mn and Co$_{n-1}$V clusters," Chem. Phys. Lett. **467**, 114–119 (2008).

[12]U. Rohrmann, S. Schäfer, and R. Schäfer, "Size- and temperature-dependent magnetic response of molecular cage clusters: Manganese-doped tin clusters," J. Phys. Chem. A **113**, 12115–12121 (2009).

[13]B.-R. Wang, Q.-M. Ma, Y. Liu, and Y.-C. Li, "Small Fe$_n$Mn clusters: Magnetic order and magnetic moment," Solid State Commun. **149**, 210–213 (2009).

[14]Y. Mu, Y. Han, J. Wang, J.-G. Wan, and G. Wang, "Structures and magnetic properties of Pd$_n$ clusters (n = 3–19) doped by Mn atoms," Phys. Rev. A **84**, 053201 (2011).

[15]M. Zhang, H. Zhang, L. Zhao, Y. Li, and Y. Luo, "Low-energy isomer identification, structural evolution, and magnetic properties in manganese-doped gold clusters MnAu$_n$ (n = 1–16)," J. Phys. Chem. A **116**, 1493–1502 (2012).

[16]G. L. Gutsev, L. E. Johnson, K. G. Belay, C. A. Weatherford, L. G. Gutsev, and B. R. Ramachandran, "Structure and magnetic properties of Fe$_{12}$X clusters," Chem. Phys. **430**, 62–68 (2014).

[17]S. Datta, M. Kabir, A. Mookerjee, and T. Saha-Dasgupta, "Engineering the magnetic properties of the Mn$_{13}$ cluster by doping," Phys. Rev. B **83**, 075425 (2011).

[18]B. K. Rao and P. Jena, "Giant magnetic moments of nitrogen-doped Mn clusters and their relevance to ferromagnetism in Mn-doped GaN," Phys. Rev. Lett. **89**, 185504 (2002).

[19]S. C. Erwin, L. Zu, M. I. Haftel, A. L. Efros, T. A. Kennedy, and D. J. Norris, "Doping semiconductor nanocrystals," Nature **436**, 91–94 (2005).

[20]T. J. Norman, D. Magana, T. Wilson, C. Burns, J. Z. Zhang, D. Cao, and F. Bridges, "Optical and surface structural properties of Mn$_2^+$-doped ZnSe nanoparticles," J. Phys. Chem. B **107**, 6309–6317 (2003).

[21]S. A. Wolf, D. D. Awschalom, R. A. Buhrman, J. M. Daughton, S. Molnár, M. L. von Roukes, A. Y. Chtchelkanova, and D. M. Treger, "Spintronics: A spin-based electronics vision for the future," Science **294**, 1488–1495 (2001).

[22]W. Zheng, Z. Wang, J. Wright, B. Goundie, N. S. Dalal, R. W. Meulenberg, and G. F. Strouse, "Probing the local site environments in Mn:CdSe quantum dots," J. Phys. Chem. C **115**, 23305–23314 (2011).

[23]Z. Wang, W. Zheng, J. van Tol, N. S. Dalal, and G. F. Strouse, "High-field electron paramagnetic resonance as a microscopic probe of anisotropic strain at Mn$_2^+$ sites in CdSe:Mn$_2^+$ quantum dots," Chem. Phys. Lett. **524**, 73–77 (2012).

[24]J. Jellinek, P. H. Acioli, J. Garciá-Rodeja, W. Zheng, O. C. Thomas, and K. H. Bowen, Jr., "Mn$_n^-$-clusters: Size-induced transition to half metallicity," Phys. Rev. B **74**, 153401 (2006).

[25]G. L. Gutsev, M. D. Mochena, C. W. Bauschlicher, Jr., W.-J. Zheng, O. C. Thomas, and K. H. Bowen, "Electronic and geometrical structure of Mn$_{13}$ anions, cations, and neutrals," J. Chem. Phys. **129**, 044310 (2008).

[26]G. M. Koretsky and M. B. Knickelbein, "Photoionization studies of manganese clusters: Ionization potentials for Mn$_7$ to Mn$_{64}$," J. Chem. Phys. **106**, 9810–9814 (1997).

[27]M. B. Knickelbein, "Experimental observation of superparamagnetism in manganese clusters," Phys. Rev. Lett. **86**, 5255–5257 (2001).

[28]M. B. Knickelbein, "Magnetic ordering in manganese clusters," Phys. Rev. B **70**, 014424 (2004).

[29]A. Terasaki, T. M. Briere, M. Kulawik, S. Minemoto, K. Tono, A. Matsushita, and T. Kondow, "Ferromagnetic spin coupling in the manganese trimer ion evidenced by photodissociation spectroscopy," J. Chem. Phys. **118**, 2180–2185 (2003).

[30]A. Terasaki, S. Minemoto, and T. Kondow, "Energetics of the manganese trimer and tetramer ions," J. Chem. Phys. **117**, 7520–7524 (2002).

[31]K. Tono, A. Terasaki, T. Ohta, and T. Kondow, "Weak metal–metal bonding in small manganese cluster ions, Mn$_N^+$ (N ≤ 7)," J. Chem. Phys. **123**, 174314 (2005).

[32]S. K. Nayak, M. Nooijen, and P. Jena, "Isomerism and novel magnetic order in Mn$_{13}$ cluster," J. Phys. Chem. A **103**, 9853–9856 (1999).

[33]T. M. Briere, M. H. F. Sluiter, V. Kumar, and Y. Kawazoe, "Atomic structures and magnetic behavior of Mn clusters," Phys. Rev. B **66**, 064412 (2002).

[34]F. López-Urías and A. Díaz-Ortiz, "Magnetism in Mn clusters: Interplay between spin ordering and structure," Phys. Rev. B **68**, 132405 (2003).

[35]R. C. Longo, J. Carrete, and L. J. Gallego, "A density-functional study of the vertical ionization potentials of the cluster Mn$_{13}$," J. Chem. Phys. **131**, 046101 (2009).

[36]M. J. Piotrowski, P. Piquini, and J. L. F. Da Silva, "Density functional theory investigation of 3d, 4d, and 5d 13-atom metal clusters," Phys. Rev. B **81**, 155446 (2010).

[37]M. J. Piotrowski, P. Piquini, M. M. Odashima, and J. L. F. Da Silva, "Transition-metal 13-atom clusters assessed with solid and surface-biased functionals," J. Chem. Phys. **134**, 134105 (2011).

[38]G. L. Gutsev, C. A. Weatherford, K. G. Belay, B. R. Ramachandran, and P. Jena, "An all-electron density functional theory study of the structure and properties of the neutral and singly charged M$_{12}$ and M$_{13}$ clusters: M = Sc–Zn," J. Chem. Phys. **138**, 164303 (2013).

[39]S. K. Nayak and P. Jena, "Anomalous magnetism in small Mn clusters," Chem. Phys. Lett. **289**, 473–479 (1998).

[40]N. O. Jones, S. N. Khanna, T. Baruah, and M. R. Pederson, "Classical Stern–Gerlach profiles of Mn$_5$ and Mn$_6$ clusters," Phys. Rev. B **70**, 045416 (2004).

[41]B. N. Papas and H. F. Schaefer III, "Homonuclear transition-metal trimers," J. Chem. Phys. **123**, 0743211 (2005).

[42]R. Sekine, R. Kondo, T. Yamamoto, and J. Onoe, "Geometric and electronic structures of Tc and Mn clusters by density functional calculations," Radiochemistry **45**, 233–236 (2003).

[43]P. Bobadova-Parvanova, K. A. Jackson, S. Srinivas, and M. Horoi, "Structure, bonding, and magnetism in manganese clusters," J. Chem. Phys. **122**, 014310 (2005).

[44]M. Kabir, D. G. Kanhere, and A. Mookerjee, "Structure, electronic properties, and magnetic transition in manganese clusters," Phys. Rev. B **73**, 224439 (2006).

[45]R. C. Longo, E. G. Noya, and L. J. Gallego, "Noncollinear magnetic order in the six-atom Mn cluster," J. Chem. Phys. **122**, 226102 (2005).

[46]R. C. Longo, E. G. Noya, and L. J. Gallego, "Fully unconstrained density-functional study of the structures and magnetic moments of small Mn$_n$ clusters (n = 2–7)," Phys. Rev. B **72**, 174409 (2005).

[47]T. Morisato, S. N. Khanna, and Y. Kawazoe, "First-principles study of the onset of noncollinearity in Mn$_n$ clusters: Magnetic arrangements in Mn$_5$ and Mn$_6$," Phys. Rev. B **72**, 014435 (2005).

[48]M. Kabir, D. G. Kanhere, and A. Mookerjee, "Emergence of noncollinear magnetic ordering in small magnetic clusters Mn$_n$ and As@Mn$_n$," Phys. Rev. B **75**, 214433 (2007).

[49]G. L. Gutsev and C. W. Bauschlicher, Jr., "Chemical bonding, electron affinity, and ionization energies of the homonuclear 3D-metal dimers," J. Phys. Chem. A **107**, 4755–4767 (2003).

[50]G. L. Gutsev, M. D. Mochena, P. Jena, C. W. Bauschlicher, Jr., and H. Partridge III, "Periodic table of 3d-metal dimers and their ions," J. Chem. Phys. **121**, 6785–6797 (2004).

[51]S. Yamanaka, T. Ukai, K. Nakata, R. Takeda, M. Shoji, T. Kawakami, T. Takada, and K. Yamaguchi, "Density functional study of manganese dimer," Int. J. Quantum Chem. **107**, 3178–3190 (2007).

[52]S. Yamamoto, H. Tatewaki, H. Moriyama, and H. Nakano, "A study of the ground state of manganese dimer using quasidegenerate perturbation theory," J. Phys. Chem. A **124**, 124302 (2006).

[53]M. S. Mona, H. Mori, and E. Miyoshi, "Theoretical study of low-lying electronic states of Mn$_2$ using a newly developed relativistic model core potential," Chem. Phys. Lett. **462**, 23–26 (2008).

[54]I. Negodaev, C. Graaf, and R. de Caballol, "On the Heisenberg behaviour of magnetic coupling in the manganese dimer," Chem. Phys. Lett. **458**, 290–294 (2008).

[55]D. Tzeli, U. Miranda, I. G. Kaplan, and A. Mavridis, "First principles study of the electronic structure and bonding of Mn_2," J. Phys. Chem. A **129**, 154310 (2008).

[56]C. Camacho, H. A. Witek, and S. Yamamoto, "Intruder states in multireference perturbation theory: The ground state of manganese dimer," J. Comput. Chem. **30**, 468–478 (2009).

[57]A. A. Buchachenko, G. M. Chałasiński, and M. M. Szcześniak, "Electronic structure and spin coupling of the manganese dimer: The state of the art of *ab initio* approach," J. Chem. Phys. **132**, 024312 (2010).

[58]M. Cheeseman, R. J. Van Zee, and W. Weltner, Jr., "Exchange striction in the Mn_2 molecule," J. Chem. Phys. **91**, 2748–2749 (1989).

[59]A. Terasaki, A. Matsushita, K. Tono, R. T. Yadav, T. M. Briere, and T. Kondow, "Electronic states of the manganese dimer ion probed by photo-dissociation spectroscopy," J. Chem. Phys. **114**, 9367–9370 (2001).

[60]R. Krishnan, J. S. Binkley, R. Seeger, and J. A. Pople, "Self-consistent molecular orbital methods. XX. A basis set for correlated wave functions," J. Chem. Phys. **72**, 650–654 (1980).

[61]A. D. Becke, "Density-functional exchange-energy approximation with correct asymptotic-behavior," Phys. Rev. A **38**, 3098–3100 (1988).

[62]J. P. Perdew and Y. Wang, "Accurate and simple analytic representation of the electron-gas correlation-energy," Phys. Rev. B **45**, 13244–13249 (1992).

[63]J. P. Perdew, J. A. Chevary, S. H. Vosko, K. A. Jackson, M. R. Pederson, D. J. Singh, and C. Fiolhais, "Atoms, molecules, solids, and surfaces: Applications of the generalized gradient approximation for exchange and correlation," Phys. Rev. B **46**, 6671–6687 (1992).

[64]C. Lee, W. Yang, and R. G. Parr, "Development of the Colle-Salvetti correlation-energy formula into a functional of the electron density," Phys. Rev. B **37**, 785–789 (1988).

[65]J. P. Perdew, K. Burke, and M. Ernzerhof, "Generalized gradient approximation made simple," Phys. Rev. Lett. **77**, 3865–3868 (1996).

[66]J. P. Perdew, S. Kurth, A. Zupan, and P. Blaha, "Accurate density functional with correct formal properties: A step beyond the generalized gradient approximation," Phys. Rev. Lett. **82**, 2544–2547 (1999).

[67]J. M. Tao, J. P. Perdew, V. N. Staroverov, and G. E. Scuseria, "Climbing the density functional ladder: Nonempirical meta-generalized gradient approximation designed for molecules and solids," Phys. Rev. Lett. **91**, 146401 (2003).

[68]A. D. Becke, "Density-functional thermochemistry. 3. The role of exact exchange," J. Chem. Phys. **98**, 5648–5652 (1993).

[69]T. Yanai, D. Tew, and N. Handy, "A new hybrid exchange–correlation functional using the Coulomb-attenuating method (CAM-B3LYP)," Chem. Phys. Lett. **393**, 51–57 (2004).

[70]J.-D. Chai and M. Head-Gordon, "Long-range corrected hybrid density functionals with damped atom–atom dispersion corrections," Phys. Chem. Chem. Phys. **10**, 6615–6620 (2008).

[71]M. J. Frisch, G. W. Trucks, H. B. Schlegel, G. E. Scuseria, M. A. Robb, J. R. Cheeseman, G. Scalmani, V. Barone, B. Mennucci, G. A. Petersson *et al.*, GAUSSIAN 09, Revision C. 01, Gaussian, Inc., Wallingford, CT, 2009.

[72]N. B. Balabanov and K. A. Peterson, "Systematically convergent basis sets for transition metals. I. All-electron correlation consistent basis sets for the 3D elements Sc–Zn," J. Chem. Phys. **123**, 064107 (2005).

[73]G. L. Gutsev and C. W. Bauschlicher, Jr., "Electron affinities, ionization energies, and fragmentation energies of Fe_n clusters (n = 2-6): A density functional theory study," J. Phys. Chem. A **107**, 7013–7023 (2003).

[74]G. L. Gutsev, C. A. Weatherford, P. Jena, E. Johnson, and B. R. Ramachandran, "Structure and properties of Fe_n, Fe_n^-, and Fe_n^+ clusters, n = 7-20," J. Phys. Chem. A **116**, 10218–10228 (2012).

[75]A. E. Reed, L. A. Curtiss, and F. Weinhold, "Intermolecular interactions from a natural bond orbital, donor-acceptor viewpoint," Chem. Rev. **88**, 899–926 (1988).

[76]S. Peredkov, M. Neeb, W. Eberhardt, J. Meyer, M. Tombers, H. Kampschulte, and G. Niedner-Schatteburg, "Spin and orbital magnetic moments of free nanoparticles," Phys. Rev. Lett. **107**, 233401 (2011).

[77]M. Niemeyer, K. Hirsch, V. Zamudio-Bayer, A. Langenberg, M. Vogel, M. Kossick, C. Ebrecht, K. Egashira, A. Terasaki, T. Möller, B. Issendorff, and J. T. von Lau, "Spin coupling and orbital angular momentum quenching in free iron clusters," Phys. Rev. Lett. **108**, 05720 (2012).

[78]A. Langenberg, K. Hirsch, A. Ławicki, V. Zamudio-Bayer, M. Niemeyer, P. Chmiela, B. Langbehn, A. Terasaki, B. Issendorff, and J. T. von Lau, "Spin and orbital magnetic moments of size-selected iron, cobalt, and nickel clusters," Phys. Rev. B **90**, 184420 (2014).

[79]H. Hotop and W. C. Lineberger, "Binding energies in atomic negative ions: II," J. Phys. Chem. Ref. Data **14**, 731–750 (1985).

[80]L.-S. Wang, X. Li, and H.-F. Zhang, "Probing the electronic structure of iron clusters using photoelectron spectroscopy," Chem. Phys. **262**, 53–63 (2000).